NISTIR 5096

Detection of Quasi-Static Electric Fields Radiated by Electrically Small Emitters

David A. Hill
Kenneth H. Cavcey

NIST

National Institute of Standards and Technology
Technology Administration, U.S. Department of Commerce

Detection of Quasi-Static Electric Fields Radiated by Electrically Small Emitters

David A. Hill
Kenneth H. Cavcey

*Electronics and Electrical Engineering Laboratory
Radio-Frequency Technology Division*

June 2000

National Institute of Justice

Jeremy Travis
Director

ABOUT THE LAW ENFORCEMENT AND CORRECTIONS
STANDARDS AND TESTING PROGRAM

The Law Enforcement and Corrections Standards and Testing Program is sponsored by the Office of Science and Technology of the National Institute of Justice (NIJ), U.S. Department of Justice. The program responds to the mandate of the Justice System Improvement Act of 1979, which created NIJ and directed it to encourage research and development to improve the criminal justice system and to disseminate the results to Federal, State, and local agencies.

The Law Enforcement and Corrections Standards and Testing Program is an applied research effort that determines the technological needs of justice system agencies, sets minimum performance standards for specific devices, tests commercially available equipment against those standards, and disseminates the standards and the test results to criminal justice agencies nationally and internationally.

The program operates through:

The *Law Enforcement and Corrections Technology Advisory Council* (LECTAC) consisting of nationally recognized criminal justice practitioners from Federal, State, and local agencies, which assesses technological needs and sets priorities for research programs and items to be evaluated and tested.

The *Office of Law Enforcement Standards* (OLES) at the National Institute of Standards and Technology, which develops voluntary national performance standards for compliance testing to ensure that individual items of equipment are suitable for use by criminal justice agencies. The standards are based upon laboratory testing and evaluation of representative samples of each item of equipment to determine the key attributes, develop test methods, and establish minimum performance requirements for each essential attribute. In addition to the highly technical standards, OLES also produces technical reports and user guidelines that explain in nontechnical terms the capabilities of available equipment.

The *National Law Enforcement and Corrections Technology Center* (NLECTC), operated by a grantee, which supervises a national compliance testing program conducted by independent laboratories. The standards developed by OLES serve as performance benchmarks against which commercial equipment is measured. The facilities, personnel, and testing capabilities of the independent laboratories are evaluated by OLES prior to testing each item of equipment, and OLES helps the NLECTC staff review and analyze data. Test results are published in Equipment Performance Reports designed to help justice system procurement officials make informed purchasing decisions.

Publications are available at no charge from the National Law Enforcement and Corrections Technology Center. Some documents are also available online through the Internet/World Wide Web. To request a document or additional information, call 800-248-2742 or 301-519-5060, or write:

National Law Enforcement and Corrections Technology Center
P.O. Box 1160
Rockville, MD 20849-1160
E-mail: *asknlectc@nlectc.org*
World Wide Web address: *http://www.nlectc.org*

CONTENTS

FOREWORD

The Office of Law Enforcement Standards (OLES) of the National Institute of Standards and Technology (NIST) furnishes technical support to the National Institute of Justice (NIJ) program to strengthen law enforcement and criminal justice in the United States. OLES's function is to conduct research that will assist law enforcement and criminal justice agencies in the selection and procurement of quality equipment.

OLES is: (1) Subjecting existing equipment to laboratory testing and evaluation, and (2) conducting research leading to the development of several series of documents, including national standards, user guides, and technical reports.

This document covers research conducted by OLES under the sponsorship of the NIJ. Additional reports as well as other documents are being issued under the OLES program in the areas of protective clothing and equipment, communications systems, emergency equipment, investigative aids, security systems, vehicles, weapons, and analytical techniques and standard reference materials used by the forensic community.

Technical comments and suggestions concerning this report are invited from all interested parties. They may be addressed to the Office of Law Enforcement Standards, National Institute of Standards and Technology, Gaithersburg, MD 20899-8102.

David G. Boyd, Director
Office of Science and Technology
National Institute of Justice

PREFACE

This is the third and final report in a three-year project on Detection of Electronic Bomb Detonators, and it covers the period from January 1999 through March 2000. The project is sponsored by the National Institute of Justice, David G. Boyd, Director, Office of Science and Technology. The research was performed by the NIST Radio-Frequency Technology Division and was monitored by A. George Lieberman, Program Manager for Communications Systems and Kathleen M. Higgins, Director of the Office of Law Enforcement Standards (OLES).

The first report on this project covered the theory of separating the fields of interest (from electronic timers) from undesired noise fields from external sources by using the techniques of spherical, near-field scanning as developed at NIST:

> Hill, D.A. Spherical-wave characterization of interior and exterior electromagnetic sources. Natl. Inst. Stand. Technol. NISTIR 5072; December 1997.

The second report on this project covered the theory and measurement techniques for determining the dipole moments of weak, electrically small emitters. The measurement technique made use of a transverse electromagnetic (TEM) cell, and it was used to determine the three orthogonal electric dipole moments of two electronic timers for frequencies from 200 kHz to 8 MHz. The magnetic dipole moments were found to be too small to measure. The practical conclusions were that electronic timers of the type that could be used in bomb detonators do radiate weak electric fields that can be measured using TEM cells that have been well characterized at NIST:

> Hill, D.A.; Cavcey, K.H. Dipole moments of weak, electrically small emitters from TEM-cell measurements. Natl. Inst. Stand. Technol. NISTIR 5079; December 1998.

The purposes of this report are (a) to present the theory for near-field detection of quasi-static electric fields produced by electrically small emitters and (b) to demonstrate detection of these fields with linear dipole and monopole antennas. These antenna types were chosen because they respond well to electric fields and they are sufficiently portable that they could be used in a search operation where the location of the small radiator (electronic timer) is unknown. Successful detection measurements of timer electric fields were achieved at a frequency of 200 kHz with both antenna types, but the detection range (10 to 20 cm) is much too short to be used in a search application. This small detection range falls below the theoretical prediction made from previous TEM-cell characterization of electronic timer radiation. One of the main reasons is that the background noise fields were larger than expected from published values. The unexpectedly large background noise fields required us to narrow the measurement bandwidth, hence reducing the desired signal and increasing the measurement uncertainty.

DETECTION OF QUASI-STATIC ELECTRIC FIELDS
RADIATED BY ELECTRICALLY SMALL EMITTERS

David A. Hill and Kenneth H. Cavcey

Radio Frequency Technology Division
National Institute of Standards and Technology
Boulder, Colorado 80303

This report presents the theory for near-field detection of quasi-static electric fields produced by electrically small emitters that radiate as small electric dipoles. The intended application is the detection of electronic timers of the type that could be used in bomb detonators. The search antenna could be either a linear dipole or a monopole antenna with a circular ground plane. Reciprocity is used to show that the induced open-circuit voltage is proportional to the electric field of the search antenna at the dipole source location when the search antenna is used in the transmitting mode. Comparison detection measurements have been made at a frequency of 200 kHz, and the measured open-circuit voltage falls below the theoretical prediction. Also, the background noise fields are higher than expected from published values. Consequently, the detection range is much shorter (10 to 20 cm) than expected, and the method does not look promising for timer search applications.

Key words: dipole moment; electrically small emitter; linear dipole antenna; monopole antenna; noise spectral density; quasi-static electric field; reciprocity.

1. INTRODUCTION

In a previous report [1], we showed that electronic timers radiate very weak quasi-static electric fields in the same manner as does an electric dipole source. The magnitudes of the electric dipole moments at low frequencies were determined using a transverse electromagnetic (TEM) cell, and no magnetic dipole moments were detectable [1]. Spherical scanning techniques [2] could be used to determine the electric dipole moments, but in a search operation we do not expect to be able to surround the timer with an array of field probes. In searching for an electronic timer of the type that could be used in a bomb detonator, a single portable antenna is a more practical search device.

The purposes of this report are (a) to present the theory for near-field detection of quasi-static electric fields [3,4] produced by electrically small emitters and (b) to demonstrate detection of these electric fields with linear dipole and monopole antennas. Reciprocity is used in the general receiving formulation in Section 2, and the mathematical details for dipole and monopole antennas are given in Sections 3 and 4. Successful timer detection measurements with dipole and monopole antennas are described in Section 5, but the detection range is found to be much too short for practical search applications.

2. RECEIVING ANTENNA THEORY

In general the analysis of the response of a receiving antenna to the nonuniform field of a near-field source is very complicated. However, for simple linear antennas at low frequencies, reciprocity and the induced electromotive force (EMF) method can be used to obtain good approximations for the open-circuit voltage induced in the receiving antenna.

2.1 Reciprocity Analysis

Reciprocity analysis is based on two source and field states that we denote as states 1 and 2. Since we are interested in the case of detecting electric dipole radiation of electronic timers with wire antennas, only electric currents and fields are required in the formulation. So the reciprocity integral relationship can be written [5]

$$\iiint_V J_2(r) \cdot E_1(r) \, \mathrm{d}V = \iiint_V J_1(r) \cdot E_2(r) \, \mathrm{d}V, \tag{1}$$

where J_1 and E_1 are the electric current density and electric field of state 1 and J_2 and E_2 are the electric current density and electric field of state 2. The time dependence of the currents and fields is $\exp(j\omega t)$. We assume that the currents radiate in free space so that no boundary surface integrals are required in eq (1).

Consider now the geometry of a linear dipole antenna and a small emitter as shown in figure 1. In state 1, the dipole antenna is radiating, and the current density J_1 can be written

$$J_1(r) = \hat{z}\delta(x)\delta(y)I_1(z), \tag{2}$$

where $\hat{z}$ is a unit vector along the axis of the antenna, δ is the Dirac delta function, and I_1 is the antenna current. In state 2, the emitter is radiating, and the current density J_2 can be written

$$J_2(r) = j\omega p_e \delta(r - r_2), \tag{3}$$

where p_e is the electric dipole moment of the emitter located at r_2. For later results, it is convenient to write the vector dipole moment in terms of its rectangular components:

$$p_e = \hat{x}p_{ex} + \hat{y}p_{ey} + \hat{z}p_{ez}. \tag{4}$$

If we substitute eqs (2) and (3) into eq (1) and perform the integrations, we obtain

$$j\omega p_e \cdot E_1(r_2) = \int_{-h}^{h} E_{2z}(z)I_1(z) \, \mathrm{d}z, \tag{5}$$

where h is the half length of the dipole antenna. Actually, the form in eq (5) applies equally to other linear antennas with only a change in the limits of integration on the right side. Except for

the thin-wire approximation, eq (5) is exact as written. However, we will later introduce approximate expressions for the current I_1 and the resultant electric field E_1.

2.2 Induced EMF Method

The induced EMF method [6] provides a convenient method for determining the induced open-circuit voltage V_{oc} of a linear antenna in terms of its transmitting current distribution and the incident electric field. For the geometry in figure 1, V_{oc} can be written [6]

$$V_{oc} = \frac{-1}{I_1(0)} \int_{-h}^{h} E_{2z}(z) I_1(z) \, dz.$$ (6)

If we substitute eq (5) into eq (6), we obtain the desired result for V_{oc}:

$$V_{oc} = -\frac{j\omega}{I_1(0)} p_e \cdot E_1(r_2).$$ (7)

In an actual evaluation of eq (7), the factor $I_1(0)$ will cancel because E_1 is proportional to $I_1(0)$.

The advantage of eq (7) is that the received voltage can be determined in terms of the transmitted electric field E_1 evaluated at the emitter location r_2. This feature of reciprocity is well known for the far-field transmitting and receiving patterns of antennas [7], but it is equally applicable to near-field applications. Since the orientation of the emitter will not be known and the measured rectangular components of p_e are nearly equal [1], a good measure of the effectiveness of an antenna in detecting a timer at a location r_2 is $|E_1(r_2)/I_1(0)|$. This quantity has units of Ω/m, and the quantity $j\omega p_e$ has units of A·m.

The induced EMF method can also be used to determine the input impedance of linear antennas [6]. When the dipole length $2h$ is small compared to the free-space wavelength λ, the imput impedance is primarily a capacitive reactance $(j\omega C_d)^{-1}$. The dipole capacitance C_d is given by [8]

$$C_d = \frac{\pi \varepsilon_0 h}{\ln(2h/d) - 1},$$ (8)

where ε_0 is the permittivity of free space and d is the wire diameter. The approximate equivalent circuit is shown in figure 2, where the small radiation resistance of the dipole antenna is neglected.

3. DIPOLE ANTENNA NEAR FIELDS

For thin dipole antennas with a length not exceeding a half wavelength, the current distribution $I(z)$ can be approximated as sinusoidal [6]:

$$I(z) = I_0 \frac{\sin[k(h-|z|)]}{\sin(kh)}, \quad |z| < h, \tag{9}$$

where I_0 equals the current at the feedpoint $I(0)$, $k = \omega\sqrt{\mu_0\varepsilon_0}$, and μ_0 is the magnetic permeability of free space. For our low-frequency application, the dipole antenna is electrically short ($kh \ll 1$) and eq (9) reduces to the following triangular distribution

$$I(z) \approx I_0\left(1 - \frac{|z|}{h}\right), \quad |z| < h. \tag{10}$$

The nonzero electric field components, E_ρ and E_z, and magnetic field component H_ϕ for the dipole current distribution in eq (9) are well known [6]. In the quasi-static approximation, we assume that both the dipole length and the distance to the field point are electrically small ($kr \ll 1$). In this case, the current distribution in eq (10) generates the following electric field components:

$$E_\rho = \frac{-I_0}{4\pi j \omega \varepsilon_0 h \rho}\left(\frac{z-h}{r_1} - \frac{2z}{r} + \frac{z+h}{r_2}\right) \tag{11}$$

and

$$E_z = \frac{I_0}{4\pi j \omega \varepsilon_0 h}\left(\frac{1}{r_1} - \frac{2}{r} + \frac{1}{r_2}\right), \tag{12}$$

where $r = \sqrt{\rho^2 + z^2}$, $r_1 = \sqrt{\rho^2 + (z-h)^2}$, and $r_2 = \sqrt{\rho^2 + (z+h)^2}$. The geometry is shown in figure 3. The main difference between the quasi-static results and the general results [6] is that there are no exponential propagation factors in eqs (11) and (12). Even though eqs (11) and (12) are quasi-static approximations, we use "=" rather than "$\approx$" here and throughout the rest of this report whenever the results are exact within the quasi-static regime. A similar expression could be derived for the magnetic field H_ϕ, but is not needed here.

3.1 On-Axis Field

In a search application, the electric field on the z axis ($\rho = 0$) is important because the axial field E_z has its largest magnitude there. The ρ component of the field E_ρ is zero on the axis, and the z component on the axis can be obtained directly from eq (12):

$$E_z\,|_{\rho=0} = \frac{I_0}{4\pi j \omega \varepsilon_0 h}\left(\frac{1}{|z-h|} - \frac{2}{|z|} + \frac{1}{|z+h|}\right). \tag{13}$$

Equation (13) can be simplified by combining terms:

$$E_z \mid_{\rho=0} = \frac{I_0 h}{2\pi j \omega \varepsilon_0 \mid z \mid (z^2 - h^2)}. \tag{14}$$

Equation (14) is actually valid for all values of z, but is physically meaningful only for $\mid z \mid > h$.

For large values of z^2/h^2, eq (14) simplifies to the expected inverse distance-cubed dependence:

$$E_z \mid_{\rho=0} \approx \frac{I_0 h}{2\pi j \omega \varepsilon_0 \mid z \mid^3}. \tag{15}$$

This agrees with the quasi-static field of a Hertzian dipole [3,4] of moment $(I_0 h)/(j\omega)$. It is even in z as expected for a symmetrical dipole antenna. The practical implication of eq (15) in a search application is that the received signal will fall off as distance cubed when the emitter is located more than a few dipole lengths from the dipole.

3.2 Broadside Field

The broadside field ($z = 0$) is also of interest in search applications because it is possible to move the center of the dipole quite close to the emitter in the $z = 0$ plane. The ρ component is zero for $z = 0$, and the z component can be obtained directly from eq (12):

$$\dot{E}_z \mid_{z=0} = \frac{I_0}{2\pi j \omega \varepsilon_0 h} \left(\frac{1}{\sqrt{\rho^2 + h^2}} - \frac{1}{\rho} \right). \tag{16}$$

For small ρ, the field varies as inverse distance.

For large values of ρ/h, the inverse distance terms cancel, and the field takes on the expected inverse distance-cubed dependence:

$$E_z \mid_{z=0} \approx \frac{-I_0 h}{4\pi j \omega \varepsilon_0 \rho^3}. \tag{17}$$

This result is similar to the on-axis result in eq (15) except that the sign is reversed and the magnitude is reduced by a factor of 2. This is quite different from the radiation field where the maximum field is in the broadside direction and a null exists on the z axis.

3.3 Near-Field Pattern

Equations (11) and (12) give expressions for E_ρ and E_z for general observation points. For $r/h \gg 1$, these equations simplify to

5

$$E_\rho \approx \frac{I_0 h}{2\pi j \omega \varepsilon_0 r^3}\left(\frac{3}{2}\sin\theta\cos\theta\right) \qquad (18)$$

and

$$E_z \approx \frac{I_0 h}{2\pi j \omega \varepsilon_0 r^3}\left(\cos^2\theta - \frac{1}{2}\sin^2\theta\right), \qquad (19)$$

where the polar angle $\theta = \tan^{-1}(\rho/z)$. The geometry is shown in figure 4.

Equations (18) and (19) have the form of r^{-3} times a function of θ. As indicated in Section 3.2, the magnitude of the electric field is the important quantity in near-field detection. Using eqs (18) and (19), we can write the magnitude of the electric field $|E|$ in the following manner

$$|E| = \sqrt{|E_\rho|^2 + |E_z|^2} \approx \left(\frac{I_0 h}{2\pi\omega\varepsilon_0 r^3}\right)P(\theta), \qquad (20)$$

where

$$P(\theta) = \sqrt{\cos^2\theta + \frac{1}{4}\sin^2\theta}. \qquad (21)$$

$P(\theta)$ can be thought of as the quasi-static field pattern of a linear dipole. It has a maximum value of 1 at $\theta = 0$ and π and a minimum value of 1/2 at $\theta = \pi/2$, and it has no nulls. This is very different from the $\sin\theta$ radiation pattern of the same dipole, which has a maximum at $\theta = \pi/2$ and nulls at $\theta = 0$ and π. Both patterns are shown in figure 5.

3.4 Two-Element Array

The usual advantages of antenna arrays [9] are high gain and the possibility of beam scanning. However, normal array design requires a significant electrical spacing between elements (on the order of a half wavelength) to produce a directive array pattern. Since that is not possible in our quasi-static search application, it is not clear that arrays offer any advantage.

However, one possible advantage of a simple two-element array is the cancellation of noise due to distant sources. (See the Appendix for expected noise characteristics.) The idea is that the near-field of an emitter is very nonuniform because of its inverse distance-cubed dependence, but the field of a distant noise source is fairly uniform (nearly a plane wave). So a two-element array with 180° phasing will nearly cancel the uniform noise signal, but should produce less cancellation of the emitter signal. This type of array is sometimes called a gradiometer [10] because it responds primarily to the gradient of the field.

The two-element, colinear array we consider is shown in figure 6. The dipole centers are separated by a distance s, and the terminal currents are $+I_0$ and $-I_0$. We again follow the reciprocity formulation of Section 2 so that we need to consider only the transmitting case. We

can use the field expressions in eqs (11) and (12) plus superposition to obtain the following expressions for the array fields:

$$E_\rho = \frac{-I_0}{4\pi j \omega \varepsilon_0 h \rho} \left\{ \left[\frac{z-h-s/2}{r_{1+}} - \frac{2(z-s/2)}{r_+} + \frac{z+h-s/2}{r_{2+}} \right] \right.$$
$$\left. - \left[\frac{z-h+s/2}{r_{1-}} - \frac{2(z+s/2)}{r_-} + \frac{z+h+s/2}{r_{2-}} \right] \right\}$$

(22)

and

$$E_z = \frac{I_0}{4\pi j \omega \varepsilon_0 h} \left[\left(\frac{1}{r_{1+}} - \frac{2}{r_+} + \frac{1}{r_{2+}} \right) - \left(\frac{1}{r_{1-}} - \frac{2}{r_-} + \frac{1}{r_{2-}} \right) \right],$$

(23)

where $r_{1+} = \sqrt{\rho^2 + (z-h-s/2)^2}$, $r_+ = \sqrt{\rho^2 + (z-s/2)^2}$, $r_{2+} = \sqrt{\rho^2 + (z+h-s/2)^2}$,

$r_{1-} = \sqrt{\rho^2 + (z-h+s/2)^2}$, $r_- = \sqrt{\rho^2 + (z+h+s/2)^2}$, and $r_{2-} = \sqrt{\rho^2 + (z+h+s/2)^2}$.

The terms in (22) and (23) tend to cancel each other, so that the field strength tends to be reduced over that of a single element. One way to see this clearly is to derive an expression for the field magnitude for large r and to compare it with the result for a single dipole in eq (20). For the condition $r/(s+h) \gg 1$, the following appoximation can be obtained from eqs (22) and (23):

$$|E| = \sqrt{|E_\rho|^2 + |E_z|^2} \approx \left[\frac{I_0 h P(\theta)}{2\pi \omega \varepsilon_0 r^3} \right] \left[\frac{3s |\cos \theta|}{r} \right],$$

(24)

where $P(\theta)$ is given by eq (21). Comparing eqs (20) and (24), we see that the array field is reduced because the second factor on the right side of eq (24) is small ($s/r \ll 1$).

To determine the amount of noise cancellation achieved by a two-element array, it is more convenient to consider the receiving case for plane-wave incidence. The geometry for a plane-wave noise field incident on the array is shown in figure 7. For incidence at an angle θ to the z axis, the open circuit voltage is the difference of two terms with slightly different phases:

$$V_{oc} = L_{eff} E_{n\theta} \sin \theta \left[\exp\left(jk \frac{s}{2} \cos \theta \right) - \exp\left(-jk \frac{s}{2} \cos \theta \right) \right],$$

(25)

where L_{eff} is the effective length of one dipole and $E_{n\theta}$ is the θ component of the electric field of the noise. For electrically short dipoles, the effective length is approximately half the physical length ($L_{eff} \approx h$). The exponentials in (25) can be approximated to yield

$$V_{oc} \approx hE_{n\theta} \sin\theta\, R_n \,, \tag{26}$$

where $R_n = jks\,\cos\theta$. We can consider R_n to be a noise reduction factor resulting from the cancellation in the array. For $\theta = 0$, total cancellation occurs, and $R_n = 0$. Even for other angles, the cancellation is effective because ks is small. For example, consider the case where $s = 1$ m and the frequency is 200 kHz (wavelength $\lambda = 1.5 \times 10^3$ m). Then ks is

$$ks = \frac{2\pi}{\lambda}s = \frac{2\pi}{1.5\times10^3\,\text{m}}1\,\text{m} \approx 4.19\times10^{-3}. \tag{27}$$

Hence this array would provide significant noise cancellation at 200 kHz, the frequency where timer emissions are significant [1].

4. MONOPOLE ANTENNA NEAR FIELDS

Linear dipole antennas have the advantages that they are simple, well characterized, and good receivers of electric fields as shown in the previous section. Their main disadvantage in a search application is that they do not have a single main beam. The quasi-static pattern in figure 5 shows broad peaks off both ends ($\theta = 0°$ and $180°$). This means that location of an emitter (timer) would have to be made by moving the search dipole and observing a stronger signal as the dipole approached the emitter. It would be faster and more convenient if the search antenna had some near-field directivity and a single pattern maximum. Since arrays are not promising for near-field directivity, another approach is needed.

A monopole antenna with a circular ground plane, as shown in figure 8, is a logical candidate because it also responds well to electric fields. In the forward half space ($z > 0$), the fields are nearly the same as those of a dipole. In the backward half space ($z < 0$), the ground screen shields and reduces the fields. (For an infinite radius a, the fields are zero for negative z and by image theory are the same as those of a dipole for positive z.) The purpose of this section is to derive expressions for the quasi-static electric field based on approximations for the monopole current and ground screen current available in the literature.

4.1 Fields of Linear Element

Since the sinusoidal current assumption is also a good approximation for the current $I_m(z)$ on the vertical monopole element [11], we can again use the linear current approximation of eq (10) for the current distribution:

$$I_m(z) \approx I_0\left(1 - \frac{z}{h}\right), \quad 0 \le z \le h, \tag{28}$$

where I_0 is the base current. Usually the electric and magnetic fields of linear current distributions are derived from the magnetic vector potential [6], but we chose to use the scalar potential to derive the quasi-static electric field because it will prove to be simpler in deriving the electric field of the ground screen currents.

The quasi-static electric field can be derived from the gradient of the scalar potential Φ:

$$E(r) = -\nabla\Phi(r). \tag{29}$$

The scalar potential is determined by the charge distribution, rather than the current distribution. In general we can determine the volume charge distribution q_v from the volume current density J by means of the continuity eq [4]

$$\nabla \cdot J(r) = -j\omega q_v(r). \tag{30}$$

The linear charge distribution q_l on the monopole can be obtained by specializing eq (30) to the linear current distribution in eq (28):

$$q_l(z) = \frac{-1}{j\omega}\frac{\partial I_m(z)}{\partial z} = \frac{I_0}{j\omega h}, \quad 0 < z \le h. \tag{31}$$

Strictly speaking, there is a point charge equal to $-I_0/(j\omega)$ at $z = 0$ due to the discontinuity in I_m at $z = 0$. However, we chose to neglect it because it will be cancelled by an equal and opposite point charge at the center of the ground screen. So the total electric field due to the total electric charge on the linear monopole and the circular ground screen will be correct.

The general expression for the scalar potential in terms of an integral of volume charge can be specialized to the following line integral

$$\Phi = \frac{1}{4\pi\varepsilon_0}\int_0^h \frac{q_l(z')}{R}dz' = \frac{I_0}{4\pi j\omega\varepsilon_0 h}\int_0^h \frac{dz'}{R}, \tag{32}$$

where $R = \sqrt{(z-z')^2 + \rho^2}$. The geometry is shown in figure 9. The integral in eq (32) can be evaluated analytically to obtain

$$\Phi = \frac{I_0}{4\pi j\omega\varepsilon_0 h}\ln\left[\frac{\sqrt{(h-z)^2+\rho^2}+h-z}{\sqrt{z^2+\rho^2}-z}\right]. \tag{33}$$

The electric field components, $E_{m\rho}$ and E_{mz}, due to the monopole are obtained from the gradient of eq (33):

$$E_{m\rho} = -\frac{\partial\Phi}{\partial\rho} = \frac{-I_0}{4\pi j\omega\varepsilon_0 h\rho}\left(\frac{z-h}{r_1} - \frac{z}{r}\right) \tag{34}$$

and

9

$$E_{mz} = -\frac{\partial \Phi}{\partial z} = \frac{I_0}{4\pi j \omega \varepsilon_0 h}\left(\frac{1}{r_1} - \frac{1}{r}\right). \tag{35}$$

These electric field results are consistent with those of the full dipole in eqs (11) and (12).

4.2 Ground Screen Currents and Fields

We assume that the ground screen shown in figure 8 is perfectly conducting and has zero thickness. The surface current has only a ρ component J_ρ which can be written as the sum of the primary surface current $J_{p\rho}$ and an edge-reflected surface current $J_{r\rho}$:

$$J_\rho(\rho) = J_{p\rho}(\rho) + J_{r\rho}(\rho). \tag{36}$$

The primary surface current is defined as the surface current for an infinite ground plane, and it is orthogonal to the primary tangential magnetic field:

$$J_{p\rho}(\rho) = -H_{p\phi}\,|_{z=0}\,. \tag{37}$$

By image theory, the primary tangential magnetic field of the monopole is equal to that of the dipole in free space. That magnetic field expression is well known [6], and the low-frequency (induction field) expression is

$$H_{p\phi}\,|_{z=0} = \frac{I_0}{2\pi h \rho}\left(\sqrt{\rho^2 + h^2} - \rho\right). \tag{38}$$

So the primary surface current on the ground screen is

$$J_{p\rho}(\rho) = \frac{-I_0}{2\pi h \rho}\left(\sqrt{\rho^2 + h^2} - \rho\right), \quad 0 \le \rho \le a. \tag{39}$$

The primary surface current at the edge of the ground screen ($\rho = a$) is

$$J_{p\rho}(a) = \frac{-I_0}{2\pi h a}\left(\sqrt{a^2 + h^2} - a\right). \tag{40}$$

The reflected surface current is unknown, but we will use the following approximate expression for an electrically small ground screen [12]

$$J_{r\rho}(\rho) = -J_{p\rho}(a)\frac{\rho}{a}, \quad 0 \le \rho \le a. \tag{41}$$

This expression has the desirable properties that it causes the total surface current to become zero at the edge of the ground screen ($\rho = a$) and it does not affect the continuity of the current

flowing between the monopole and the ground screen at the origin ($\rho = z = 0$). The first property eliminates the ring charge at the edge of the ground screen, and the second property avoids having a point charge at the junction of the monopole and the ground screen.

The surface charge density q_s on the ground screen can be determined by taking the surface divergence of the ground screen surface current

$$q_s = \frac{-1}{j\omega}\nabla_s \cdot J = \frac{-1}{j\omega}\frac{1}{\rho}\frac{\partial}{\partial\rho}(\rho J_\rho), \tag{42}$$

where J_ρ is given by eqs (36), (39), and (41). Substitution of J_ρ into eq (42) yields

$$q_s = \frac{I_0}{j\omega 2\pi h}\left[\frac{1}{\sqrt{\rho^2 + h^2}} - \frac{1}{\rho} - \frac{2}{a^2}\left(\sqrt{a^2 + h^2} - a\right)\right], \quad 0 \le \rho \le a. \tag{43}$$

Strictly speaking, there is also a point charge equal to $I_0/(j\omega)$ at $\rho = 0$, but we chose to neglect it because it is the negative of the point charge that occurs at the base of the monopole. Both point charges are artifacts of breaking the total antenna current distribution into two parts (the monopole and the ground screen) rather than applying the continuity equation to the entire continuous current distribution.

It is interesting to integrate the surface charge density q_s over the ground screen surface to determine the total charge Q_s on the ground screen:

$$Q_s = \int_0^{2\pi}\int_0^a q_s(\rho)\rho\,d\rho\,d\phi. \tag{44}$$

If we substitute eq (43) into eq (44), the ϕ integration contributes a factor of 2π, and the ρ integration can be carried out analytically to yield

$$Q_s = \frac{-I_0}{j\omega}. \tag{45}$$

For comparison, the total charge Q_l on the linear monopole element can be written as a line integral:

$$Q_l = \int_0^h q_l(z)\,dz = \frac{I_0}{j\omega}. \tag{46}$$

Hence the total charge on the monopole antenna is zero:

$$Q_l + Q_s = 0. \tag{47}$$

11

This is the expected result and serves as a consistency check on the approximate theory for the ground screen charge. Thus, at large distances, the monopole antenna radiates as two separated charges of opposite polarity (essentially a dipole antenna).

An accurate calculation of the monopole capacitance C_m would require a numerical method, but we can make a rough estimate from limiting cases. For a very large ground screen ($a/h \gg 1$), image theory can be used to show that the monopole capacitance approaches twice the dipole capacitance [13]

$$\lim_{a \to \infty} C_m = 2C_d , \tag{48}$$

where C_d is given by eq (8). Method-of-moments calculations [12] show that the dipole capacitance decreases as the ground screen radius decreases. (For $a = 0$, $C_m = 0$.) We are not interested in very small ground screens because the purpose of using a monopole antenna is to shield the field in the back direction. To estimate the monopole capacitance, it is useful to study the charge distribution on the ground screen. A radial charge density, $q_{s\rho} \equiv 2\pi\rho q_s$, where q_s is given by eq (43), is the more relevant quantity because its integral over ρ gives the total charge:

$$\int_0^a q_{s\rho} \, d\rho = Q_s . \tag{49}$$

The radial charge densities are shown in figure 10 for an infinite screen ($a = \infty$) and a screen of practical size ($a = h$). Because the charge density for the finite-size screen is more concentrated, its capacitance will be smaller. A rough assumption based on figure 10 is that the monopole capacitance for $a \approx h$ is approximately equal to the dipole capacitance (which is half the value for an infinite screen). The precise value of C_m will turn out not to be important in the detection application.

The electric field of the monopole antenna is important in the detection application, and the electric field of the vertical monopole element has already been given. To determine the electric field of the ground screen, the scalar potential Φ_s due to the ground screen charge can be written as the following surface integral

$$\Phi_s = \frac{1}{2\pi\varepsilon_0} \int_0^\pi \int_0^a \frac{q_s(\rho')}{R_s} \rho' \, d\rho' \, d\phi' , \tag{50}$$

where $R_s = \sqrt{\rho^2 + \rho'^2 - 2\rho\rho' \cos\phi' + z^2}$. The geometry is shown in figure 11. Since Φ_s is independent of ϕ, we have chosen to evaluate it at $\phi = 0$. We have also made use of the property that the integrand is even in ϕ'. The electric field E_s of the ground screen is given by the gradient

$$E_s = -\nabla\Phi_s = -\hat{\rho}\frac{\partial\Phi_s}{\partial\rho} - \hat{z}\frac{\partial\Phi_s}{\partial z} . \tag{51}$$

Thus the ρ and z components of the electric field are

$$E_{s\rho} = \frac{1}{2\pi\varepsilon_0} \int_0^\pi \int_0^a \frac{(\rho - \rho'\cos\phi')q_s(\rho')}{R_s^3} \rho'\,d\rho'\,d\phi' \tag{52}$$

and

$$E_{sz} = \frac{1}{2\pi\varepsilon_0} \int_0^\pi \int_0^a \frac{zq_s}{R_s^3} \rho'\,d\rho'\,d\phi'. \tag{53}$$

The ϕ integrals in eqs (50), (52), and (53) can be identified as elliptic integrals [14] that cannot be expressed in terms of elementary functions. Probably the best way to evaluate $E_{s\rho}$ and E_{sz} for general observation points would be to perform the double integrations in eqs (52) and (53) numerically. Fortunately, we can evaluate the electric field components on the z axis analytically, and this is sufficient in determining the front-to-back performance of the monopole antenna.

4.3 On-Axis Field

The on-axis case ($\rho = 0$) simplifies because $E_{s\rho} = 0$ and the integrand in eq (50) is independent of ϕ. Consequently the potential in eq (50) simplifies to

$$\Phi_s = \frac{1}{2\varepsilon_0} \int_0^a \frac{q_s(\rho')}{\sqrt{\rho'^2 + z^2}} \rho'\,d\rho'. \tag{54}$$

The evaluation of the ρ' integration is more involved because of the three terms in q_s and the square root in the denominator. However, we can break up Φ_s into three corresponding terms and evaluate each integral analytically:

$$\Phi_s = \Phi_{s1} + \Phi_{s2} + \Phi_{s3}, \tag{55}$$

where

$$\Phi_{s1} = \frac{I_0}{4\pi j \omega\varepsilon_0 h} \ln\left[\frac{\left(\sqrt{(a^2+h^2)(a^2+z^2)} + 2a^2 + h^2 + z^2\right)^{1/2}}{h + |z|} \right], \tag{56}$$

$$\Phi_{s2} = \frac{I_0}{4\pi j \omega\varepsilon_0 h} \ln\left[\frac{|z|}{a + \sqrt{a^2+z^2}} \right], \tag{57}$$

and

$$\Phi_{s3} = \frac{I_0}{2\pi j \omega\varepsilon_0 ha} \left(\sqrt{a^2+h^2} - a\right)\left(|z| - \sqrt{a^2+z^2}\right). \tag{58}$$

13

The individual terms and the total potential are even in z.

Since the z component of the electric field E_{sz} is determined from the negative of the z derivative of eq (55), it can also be written as the sum of three terms:

$$E_{sz} = E_{s1z} + E_{s2z} + E_{s3z},$$ (59)

where

$$E_{s1z} = \frac{-I_0}{4\pi j \omega \varepsilon_0 h} \left\{ \frac{z\left[\sqrt{(a^2+h^2)/(a^2+z^2)}+2\right]}{2\left[\sqrt{(a^2+h^2)(a^2+z^2)}+2a^2+h^2+z^2\right]} - \frac{\text{sgn}(z)}{h+|z|} \right\},$$ (60)

$$E_{s2z} = \frac{-I_0}{4\pi j \omega \varepsilon_0 h} \left[\frac{1}{z} - \frac{z}{\left(a+\sqrt{a^2+z^2}\right)\sqrt{a^2+z^2}} \right],$$ (61)

$$E_{s3z} = \frac{I_0}{2\pi j \omega \varepsilon_0 h a^2} \left(\sqrt{a^2+h^2}-a\right)\left[\frac{z}{\sqrt{a^2+z^2}} - \text{sgn}(z) \right],$$ (62)

and sgn(z) indicates the sign of z. The individual electric field terms in eqs (60) through (62) and hence their sum in eq (59) are odd in z.

A good check on eqs (59) through (62) is to let the radius a equal infinity:

$$E_{sz}\,|_{a=\infty} = \frac{I_0}{4\pi j \omega \varepsilon_0 h} \left[\frac{1}{z+\text{sgn}(z)h} - \frac{1}{z} \right].$$ (63)

If we add eqs (35) and (63), we obtain the total electric field of the monopole antenna on the z axis:

$$E_{mz} + E_{sz}\,|_{a=\infty} = \frac{I_0}{4\pi j \omega \varepsilon_0 h} \begin{cases} \dfrac{1}{|z-h|} - \dfrac{2}{z} + \dfrac{1}{z+h}, & z>0 \\[2mm] 0, & z<0 \end{cases}.$$ (64)

For positive z, this result agrees with the field of a dipole in eq (12). For negative z, the field is zero since it is totally shielded by the infinitely large ground screen. In the following section, we take a further look at the difference in the front ($z > 0$) and back ($z < 0$) fields for ground screens of finite radius.

4.4 Comparison of Front and Back Fields

On the z axis, the monopole field has only a z component, which is given by

$$E_{mz} = \frac{I_0}{4\pi j\omega\varepsilon_0 h}\left(\frac{1}{|z-h|} - \frac{1}{|z|}\right).$$ (65)

The total field also has only a z component, $E_{tz} = E_{mz} + E_{sz}$, where E_{mz} is given by eq (65) and E_{sz} is given by eq (59). We first look at the field close to the antenna. In the front direction (positive z), the leading term for z slightly greater than h is the first term in eq (65):

$$\lim_{z\to h^+} E_{tz} = \frac{I_0}{4\pi j\omega\varepsilon_0 h(z-h)}.$$ (66)

Hence the field is singular at the tip of the monopole.

In the back direction (negative z), the singularity for $z \to 0^-$ in eq (65) is canceled by the singularity in eq (61). So the leading term for small negative z is a constant:

$$\lim_{z\to 0^-} E_{tz} = \frac{I_0}{2\pi j\omega\varepsilon_0 h a^2}\left(\sqrt{a^2+h^2} - a\right).$$ (67)

For a small ground screen ($a/h \ll 1$), eq (67) can be approximated

$$\lim_{z\to 0^-} E_{tz} \approx \frac{I_0}{2\pi j\omega\varepsilon_0 a^2}.$$ (68)

For a large ground screen ($a/h \gg 1$), the increased shielding reduces the approximation in eq (68) by a factor $h/(2a)$:

$$\lim_{z\to 0^-} E_{tz} \approx \frac{I_0 h}{4\pi j\omega\varepsilon_0 a^3}.$$ (69)

The practical implication for a close-in search from eqs (66) and (67) is that the strongest signal will be obtained when the monopole tip approaches the electronic timer.

We look now at E_{tz} on the z axis at large distances ($|z|/h$ and $|z|/a \gg 1$) from the antenna. If we retain the first two terms in inverse powers of z, we obtain the following approximation

$$E_{tz} \approx \frac{I_0 h}{4\pi j\omega\varepsilon_0 |z|^3}\left[1 + \frac{C_4}{z}\right],$$ (70)

where

$$C_4 = \frac{1}{4h^2}\left[(a^2 + 4h^2)\sqrt{a^2+h^2} - a^3\right].$$ (71)

15

The $|z|^{-3}$ term in eq (70) can be identified as the field of a short (Hertzian) dipole of current moment $I_0 h/2$. The additional term is due to the extended current distribution on the monopole and the ground screen. For a small screen ($a/h << 1$), the additional term is proportional to the monopole length:

$$C_4 \approx h. \tag{72}$$

For a large screen ($a/h >> 1$), the additional term is proportional to the screen radius:

$$C_4 \approx a. \tag{73}$$

Since C_4 is always positive, the C_4/z term in eq (70) adds to the leading term in the forward (positive z) direction, and subtracts in the back (negative z) direction. So the monopole antenna radiates (or receives) more strongly in the forward direction, but the relative difference between the forward and back radiation decreases as $|z|$ increases.

5. DETECTION MEASURMENTS

We performed detection measurements using both a linear dipole receiving antenna and a monopole antenna with a circular ground plane. In both cases, the source was an electronic timer whose radiation characteristics (electric dipole moments) had been measured in a TEM cell [1].

5.1 Linear Dipole Receiving Antenna

For our receiving antenna, we constructed a linear dipole of length 1 m. Since the electronic timer radiates a weak, quasi-static electric field, we designed a high-gain, high-input-impedance amplifier for the detector of the antenna gap voltage. The amplifier matched the high input impedance of the dipole to the 50 Ω impedance of the spectrum analyzer, and the amplifier gain was on the order of 50 dB. To calibrate the combination of the dipole antenna and the amplifier, we used the large NIST TEM cell to generate a known electric field [15] incident on our linear dipole antenna.

Because of the weak timer fields [1], we found it necessary to perform the detection measurements in the underground control room of the NIST open area test site to reduce the competing background noise fields. Even in this environment, the noise fields were higher than expected [16-18]. We performed detection range measurements in both the broadside and end directions from the receiving dipole. Both sets of measurements were performed at a center frequency of 200 kHz with a bandwidth of 10 kHz. The noise environment placed limitations on both the center frequency and the bandwidth that had not been a problem with our earlier timer characterization in a shielded TEM cell [1].

The geometry for the broadside measurements is shown in figure 12. The timer was located in the $z = 0$ plane with the display face perpendicular to the z axis. The timer dimensions are 6.05 cm × 6.05 cm × 0.85 cm. For this orientation, only the z-directed dipole moment p_{ez} couples to the receiving dipole, as indicated by eq (7). Both the measured and theoretical open-circuit voltages are shown in figure 13 as a function of broadside distance ρ. The theoretical curve is determined from eqs (7) and (12). The previously measured value of p_{ez} [1] was

determined to be 25.2 fC·cm for a bandwidth of 100 kHz, rather than 10 kHz as used in the field measurement in figure 13. To convert to an equivalent value of p_{ez} for calculation of the theoretical curve, we make the coherent assumption that we should divide the measured value of p_{ez} by the bandwidth ratio of 10. This assumption might well be part of the reason for the offset between the measured and calculated curves in figure 13 since we do not really know the detailed spectral characteristics over the full 100 kHz bandwidth. At least the shapes of the two curves as a function of ρ are in good agreement.

The noise floor in figure 13 is determined from the measured open-circuit voltage in the absence of the timer. This noise is due primarily to external sources rather than system noise. From our calibrated antenna and amplifier, we have determined that the equivalent noise spectral density [16] has a value of 0.578 μV/(m·Hz$^{1/2}$). As indicated in the Appendix, this value is about a factor of 5 above the expected published value. This is particularly surprising since the underground location is known to provide some shielding from the above-ground fields. This high value is one of the reasons that our detection range is less than expected.

The geometry for the end measurements is shown in figure 14. The same timer was located on the z axis with the display face perpendicular to the z axis. Again, only the z-directed dipole moment p_{ez} couples to the receiving dipole, as indicated by eq (7). Both the measured and theoretical open-circuit voltages are shown in figure 15 as a function of z. (The end of the dipole is at $z = 50$ cm.) We again converted the value of p_{ez} measured in the TEM cell for a 100 kHz bandwidth to an estimated value for a 10 kHz bandwidth by dividing by 10. The theoretical curve for the open-circuit voltage again lies above the measured curve, bringing into question the bandwidth correction. The shapes of the two curves as a function of z are in good agreement.

The noise floor is higher in this case, probably because the receiving antenna was oriented differently to scan the timer position off the end. In this case the equivalent noise spectral density is 1.122 μV/(m·Hz$^{1/2}$), about a factor of 10 above the expected published value [16]. Consequently, the detection range is even less than that for the broadside measurement.

5.2 Monopole Receiving Antenna

We also constructed a monopole receiving antenna with a ground plane radius of 36 cm and a monopole length of 35 cm. We used the same high-gain amplifier as we used with the dipole antenna and mounted it below the ground plane. To calibrate the combination of the monopole antenna and the amplifier, we again used the large NIST TEM cell to generate a known electric field [15] incident on the monopole antenna. We again performed the detection measurements in the underground control room of the NIST open area test site to reduce the competing noise fields.

The geometry for these measurements is shown in figure 16. The same timer was located on the z axis with the display face perpendicular to the z axis. Again, only the z-directed dipole moment p_{ez} couples to the monopole antenna. Both the measured and theoretical open-circuit voltages are shown in figure 17 as a function of z. (The end of the monopole is at $z = 35$ cm.) The theoretical curve is calculated from eqs (7), (35), and (59). The measurements were performed at a frequency of 200 kHz, and we used the same reduced value of the dipole moment to account for the 10 kHz bandwidth. As with the dipole results, the theoretical curve lies well above the measured curve, but the shapes of the curves are in approximate agreement. The noise floor is also shown, and it again represents a noise spectral density that is above the published value [16]. Consequently, the detection range is again very small.

17

We have not performed uncertainty analyses for the detection measurements with either the dipole or the monopole receiving antenna. Well established dipole and monopole calibration measurements performed on the open area test site at NIST have expanded uncertainties (with a coverage factor of 2) of approximately 1 dB. These timer detection measurements have larger uncertainties because of the multipath environment of the underground control room and the weak, broadband radiation of the electronic timer.

6. CONCLUSIONS

We have developed the theory for the near-field detection of electric-dipole emitters using general receiving antennas. The use of reciprocity theory and the induced EMF method shows that the important quantity for the receiving antenna is the electric field that the same antenna would generate at the emitter location when the antenna is operated in the transmitting mode. The mathematical result is shown in eq (7), and this form is generally easier to evaluate than the open-circuit voltage when the receiving antenna is illuminated by a quasi-static, nonuniform field produced by an electric-dipole emitter. The particular expressions of the transmitted electric field are derived for dipole and monopole antennas and a two-element dipole array. The interesting result for both the dipole and monopole antennas is that the strongest quasi-static electric field is produced off the end of the linear element, rather than in the broadside direction where the far field is maximized.

We constructed both dipole and monopole antennas and performed detection experiments for an electronic timer of the type that could be used in a bomb detonator. The experiments at 200 kHz showed that the timer electric field could be detected, but that the detection range is too short (approximately 10 to 20 cm) for practical search applications. Part of the reason for the short detection range is that the background noise fields were larger than expected [16]. This was not an issue in our earlier characterization of electronic timers in TEM cells [1] which provide excellent shielding from external noise sources. Consequently, we conclude that an inspection system (as for baggage) would be feasible using a large TEM cell, but that a timer search method using a portable antenna is probably not feasible in a real-world noise environment.

7. REFERENCES

[1]   Hill, D.A.; Cavcey, K.H. Dipole moments of weak, electrically small emitters from TEM-cell measurements. Natl. Inst. Stand. Technol. Interagency Report 5079; 1998.

[2]   Hill, D.A. Spherical-wave characterization of interior and exterior electromagnetic sources. Natl. Inst. Stand. Technol. Interagency Report 5072; 1997.

[3]   Stratton, J.A. *Electromagnetic Theory*. New York: McGraw-Hill; 1941.

[4]   Harrington, R.F. *Time-Harmonic Electromagnetic Fields*. New York: McGraw-Hill; 1961.

[5] Monteath, G.D. *Applications of the Electromagnetic Reciprocity Principle.* Oxford: Pergamon Press; 1973.

[6] Jordan, E.C.; Balmain, K.G. *Electromagnetic Waves and Radiating Systems.* Englewood Cliffs, NJ: Prentice Hall; 1968.

[7] Park, P.K.; Tai, C.T. Receiving antennas. Ch. 6 in *Antenna Handbook* (ed., Y.T. and S.W. Lee). New York: Van Nostrand Reinhold Co.; 1988.

[8] Schelkunoff, S.A.; Friss, H.T. *Antennas, Theory and Practice.* New York: Wiley; 1952.

[9] Ma, M.T. *Theory and Application of Antenna Arrays.* New York: Wiley, 1974.

[10] Hill, D.A. Gradiometer antennas for detection of long subsurface conductors. *J. Electromagnetic Waves Applications, 8*: 237-248; 1994.

[11] Weiner, M.M. Monopole element at the center of a circular ground plane whose radius is small or comparable to a wavelength. *IEEE Trans. Antennas Propagat., 35*: 488-495; 1987.

[12] Awadalla, K.H.; Maclean, T.S. Monopole antenna at the center of circular ground plane: input impedance and radiation pattern. *IEEE Trans. Antennas Propagat., 27*: 151-153; 1979.

[13] Camell, D.G.; Larsen, E.B.; Cruz, J.E.; Hill, D.A. NIST calibration procedure for vertically polarized monopole antennas, 30 kHz to 300 MHz. Natl. Inst. Stand. Technol. Technical Note 1347; 1991.

[14] Abramowitz, M.; Stegun, I.A. *Handbook of Mathematical Functions.* Nat. Bur. Stand. (U.S.) AMS 55; 1964.

[15] Kanda, M.; Orr, R.D. Generation of standard electromagnetic fields in a TEM cell. Nat. Bur. Stand. (U.S.) Technical Note 1319; 1988.

[16] Smith, Jr., A.A. *Radio Frequency Principles and Applications.* Piscataway, NJ: IEEE Press; 1998.

[17] Characteristics and applications of atmospheric radio noise data. International Radio Consultative Committee Report 322-3: Geneva, Switzerland; 1988.

[18] Fischer, W.H. The radio noise spectrum from e.l.f. to e.h.f. *J. Atmos. Terr. Phys., 27*; 475-480; 1965.

APPENDIX: NOISE ENVIRONMENT

The external noise environment limits the sensitivity of any external electromagnetic field measurement. Noise fields can be expressed in a variety of quantities and units. Since they are all related [16], it is possible to convert noise data to the most convenient quantity. The most convenient noise quantity for our application of electric field measurement is the *noise field spectral intensity*, which has units of $V/(m \cdot Hz^{1/2})$. It is normally designated by the symbol e_n, and the electric field strength e_B within a bandwidth B is given by

$$e_B = e_n \sqrt{B}, \tag{A1}$$

where the bandwidth is given in hertz. Many noise measurements and surveys have been performed over a large range of frequencies [17,18]. In our frequency range of interest (approximately 200 kHz to 8 MHz), both man-made noise and atmospheric noise (due to worldwide lightning) are significant.

Even though both types of noise are highly variable in time and space, a typical value for the noise field spectral intensity at 200 kHz is $e_n \approx 0.1 \ \mu V/(m \cdot Hz^{1/2})$. Our previous measurements and calculations of electric fields radiated by electronic timers [1] used a 100 kHz bandwidth. So the electric field noise strength at 200 kHz in the same 100 kHz bandwidth is

$$e_B \approx 0.1 \mu V /(m \cdot Hz^{1/2}) \times \sqrt{100 \, kHz} \approx 30 \, \mu V / m. \tag{A2}$$

Both man-made and atmospheric noise decrease with frequency. However, the timer radiation decreases more rapidly with frequency so that the detection range decreases with frequency.
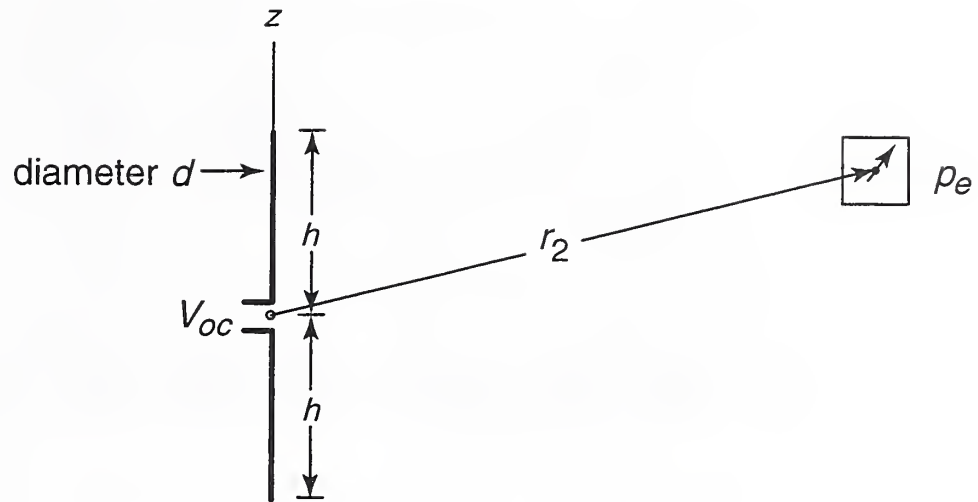
Figure 1. Dipole receiving antenna of length *2h* in the presence of an electrically small source of dipole moment p_e.
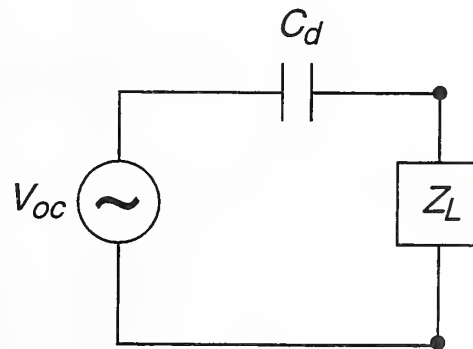
Figure 2. Equivalent circuit for a dipole antenna with capacitance C_d and load impedance Z_L.
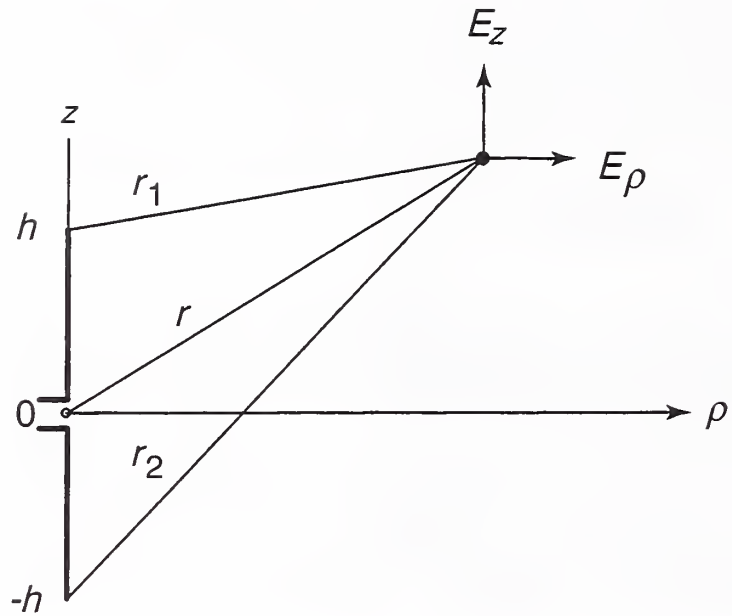
Figure 3. Geometry for the electric fields radiated by a dipole antenna of length 2h.
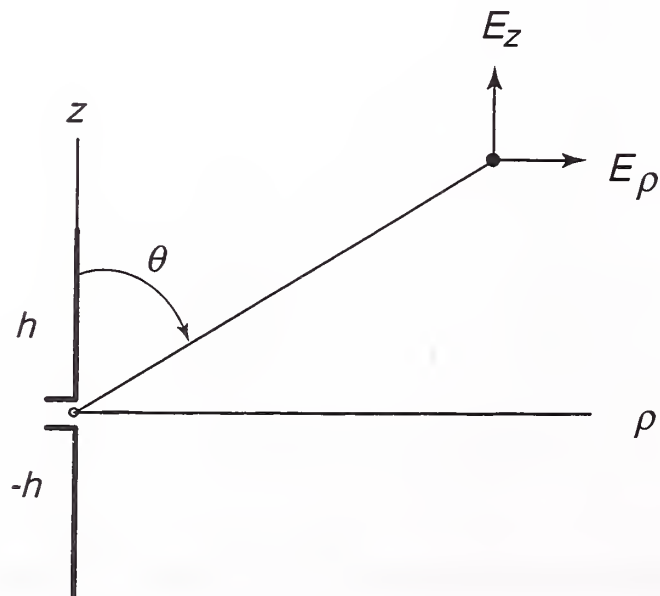
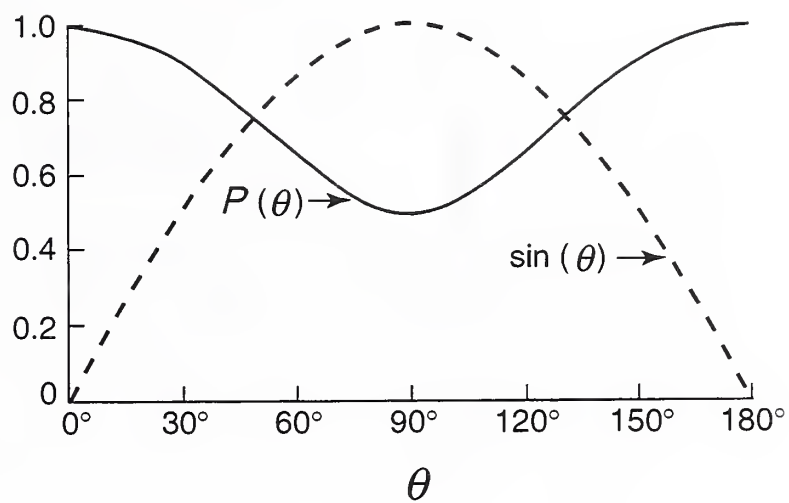Figure 4. Geometry for the near-field pattern of a dipole antenna.

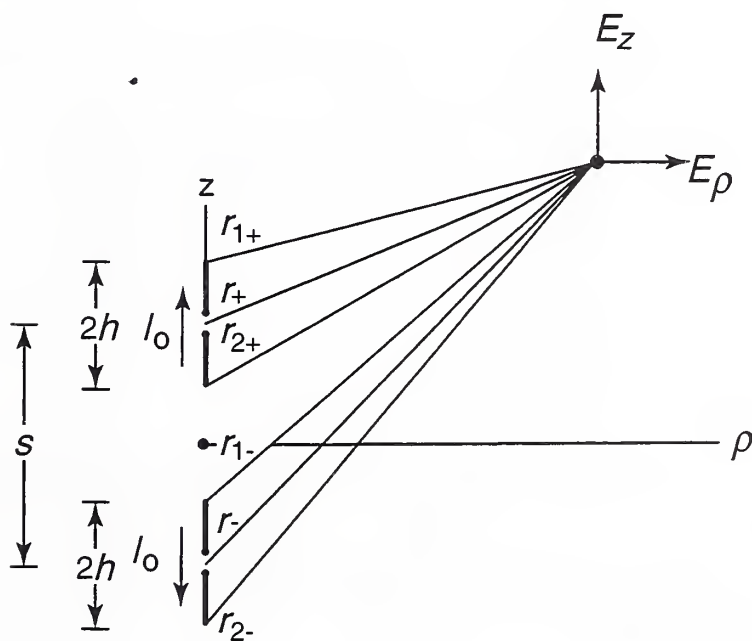Figure 5. Quasi-static field pattern $P(\theta)$ of a linear dipole compared with $\sin\theta$ far-field pattern.

Figure 6. Fields of a two-element, colinear array of dipole antennas fed 180° out of phase.
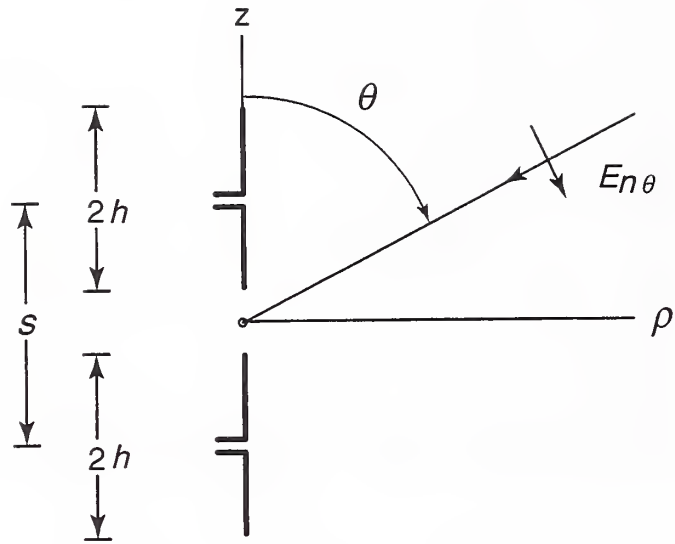
Figure 7. Plane wave field incident on a two-element, linear array of dipole antennas designed for noise cancellation.
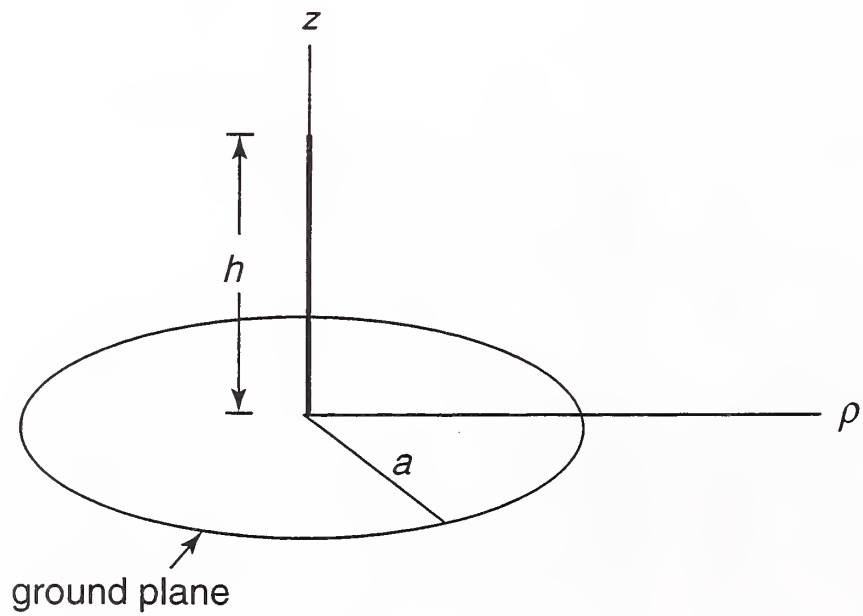
Figure 8. Monopole antenna of length h with a circular ground screen of radius a.
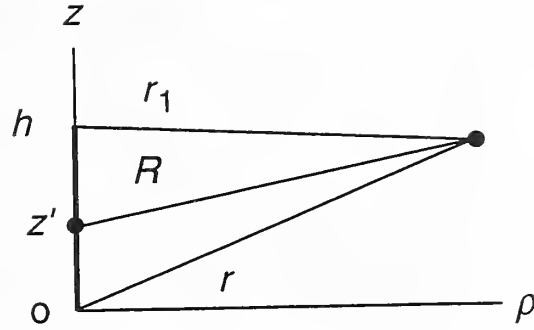
Figure 9. Geometry for fields of a linear monopole of length h.
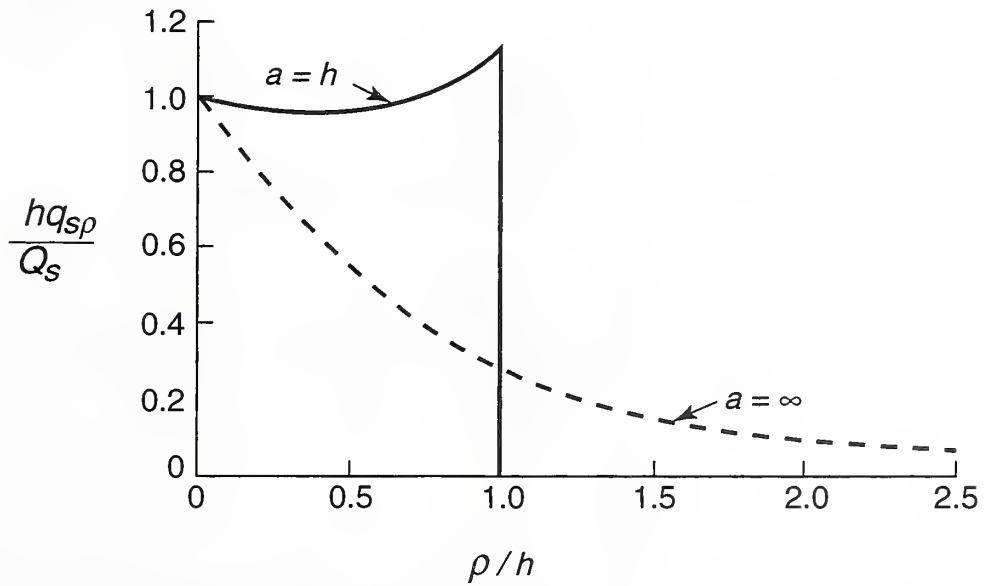
Figure 10. Radial charge density $q_{s\rho}$ on a finite ground screen ($a = h$) and an infinite ground screen ($a = \infty$).
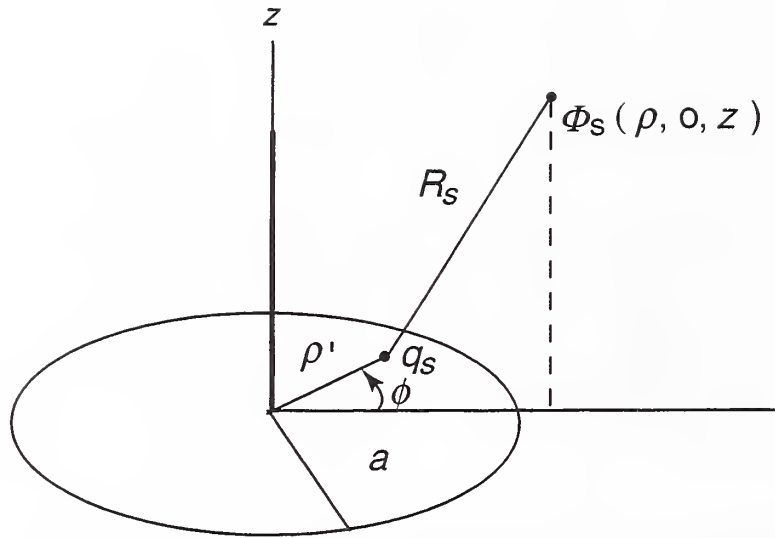
Figure 11. Geometry for the scalar potential Φ_s of the charge q_s on a circular ground screen.
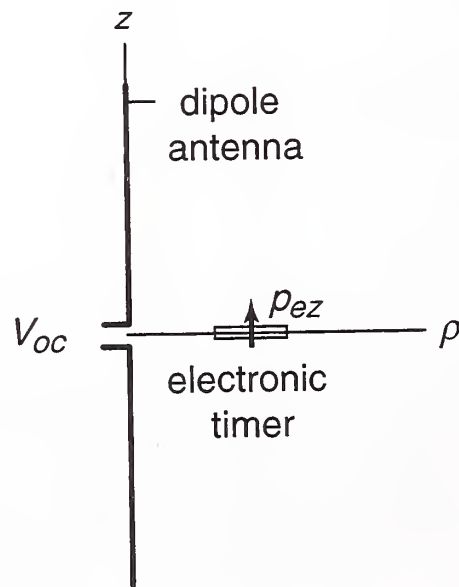
Figure 12. Geometry for an electronic timer located in the broadside direction from a linear dipole receiving antenna.
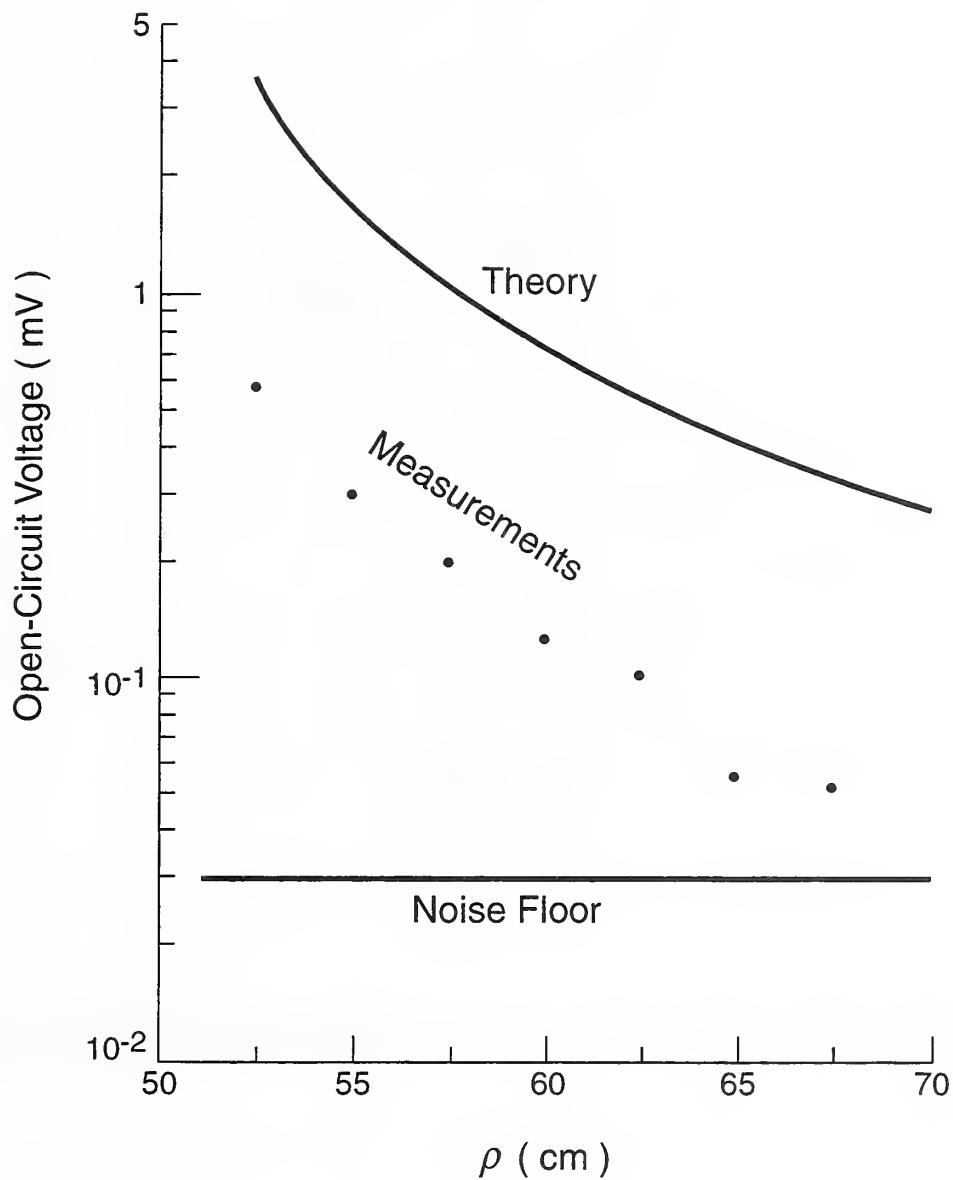
Figure 13. Theory and measurements at 200 kHz for the open-circuit voltage induced in a linear dipole antenna when an electronic timer is located at a distance ρ in the broadside direction. The measured noise floor (in the absence of the timer) is also shown.
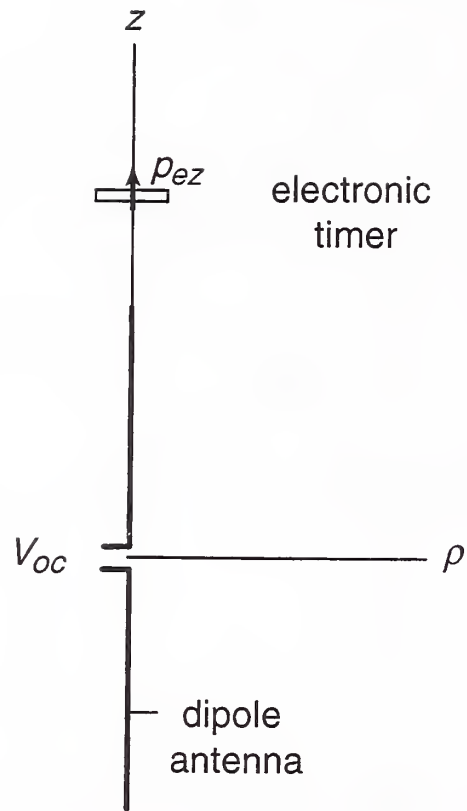
Figure 14. Geometry for an electronic timer located off the end of a linear dipole receiving antenna.
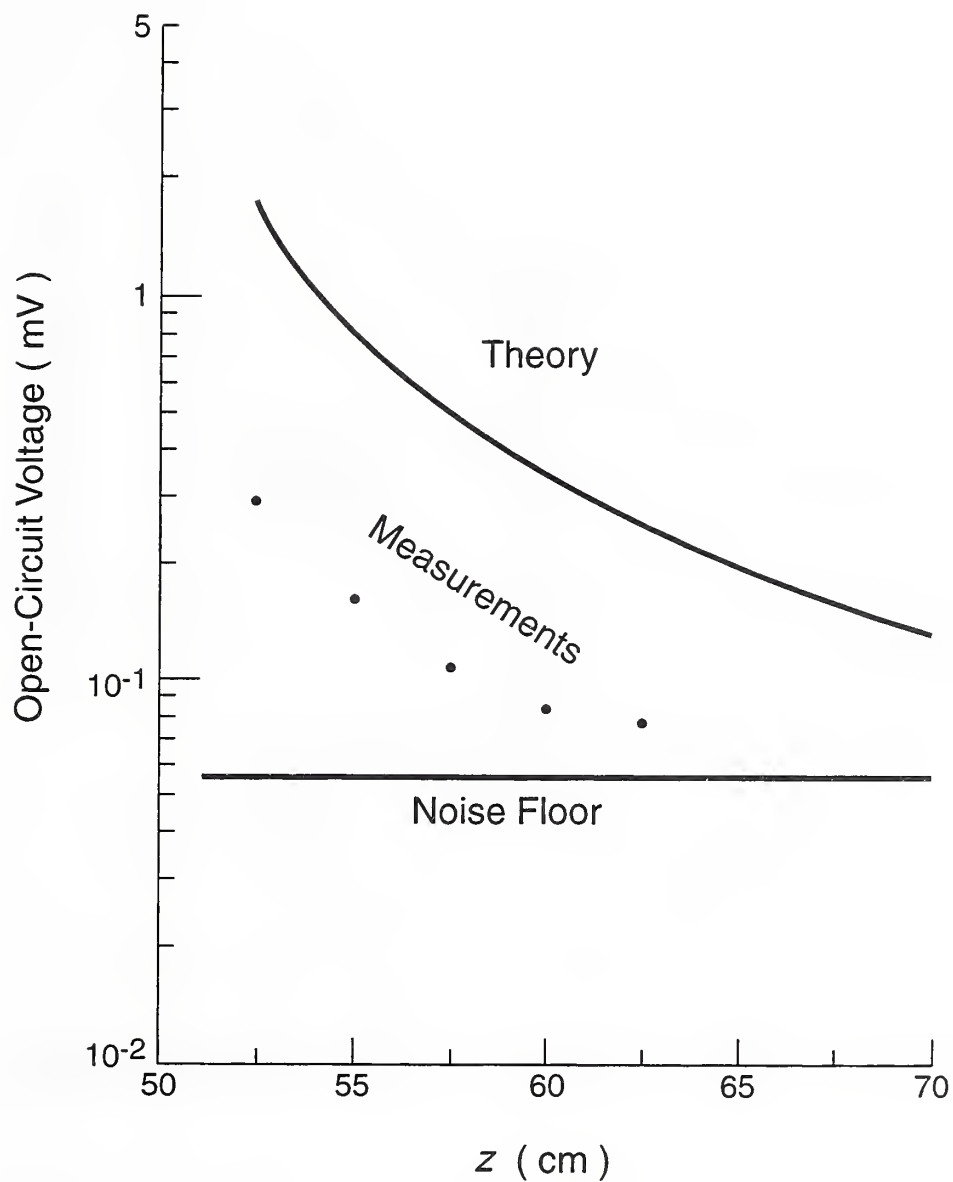
Figure 15. Theory and measurements at 200 kHz for the open-circuit voltage induced in a linear dipole antenna when an electronic timer is located off the end at a distance z from the dipole feed point. The measured noise floor (in the absence of the timer) is also shown.
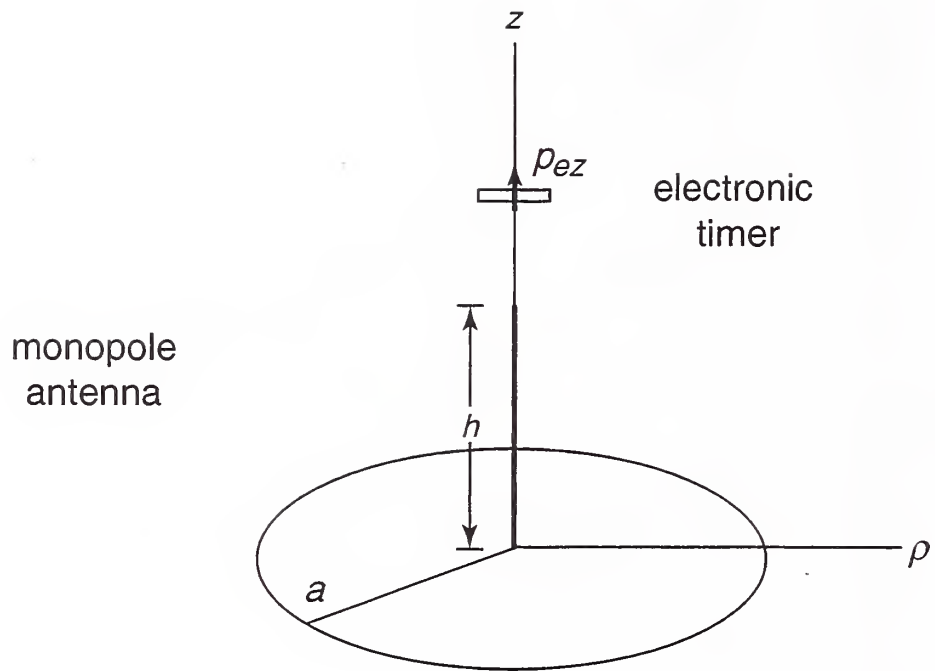
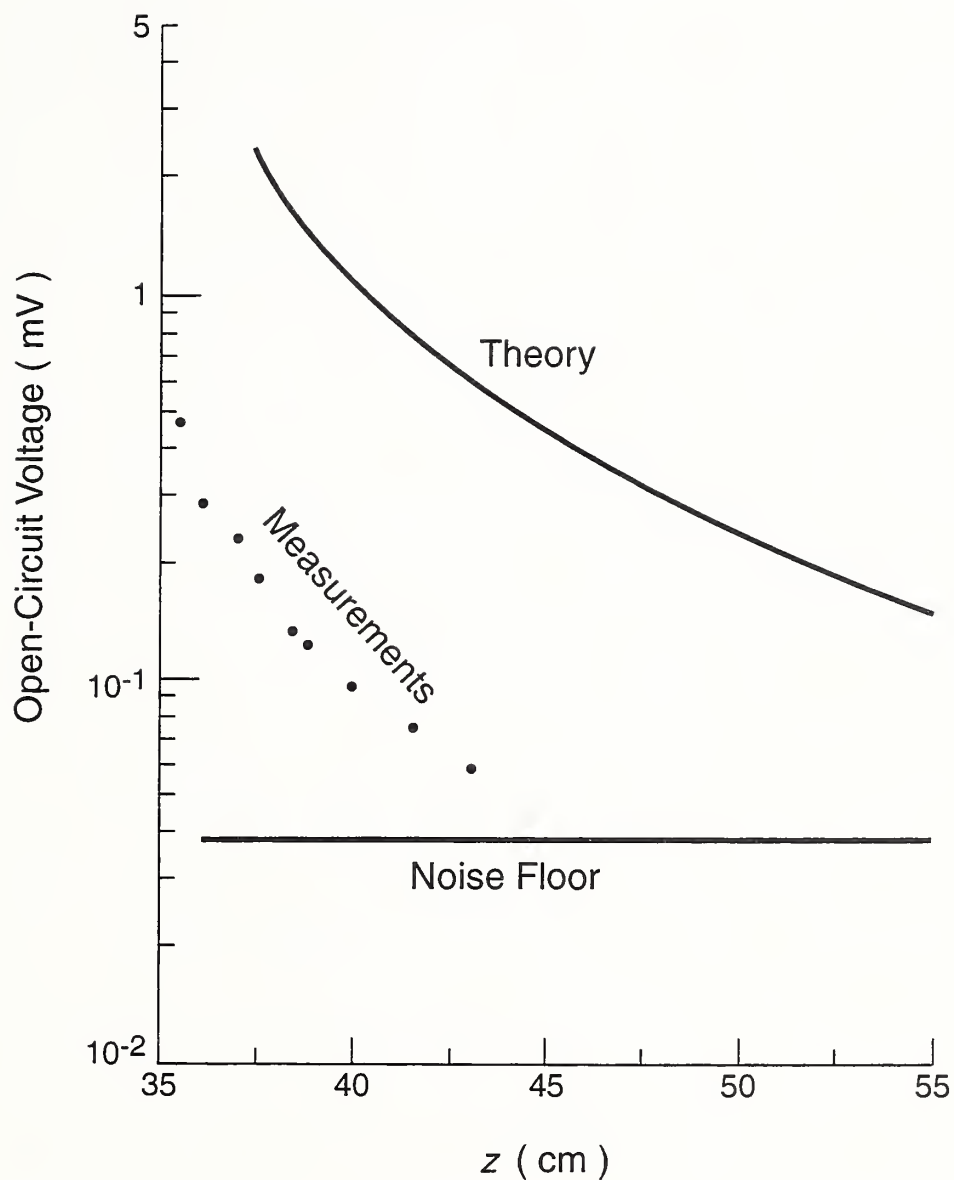Figure 16. Geometry for an electronic timer located off the end of a monopole receiving antenna.

Figure 17. Theory and measurements at 200 kHz for the open-circuit voltage induced in a monopole receiving antenna when an electronic timer is located off the end at a distance z from the monopole feed point. The measured noise floor (in the absence of the timer) is also shown.